Int J Thermophys
DOI 10.1007/s10765-012-1328-4

Digital Image Processing Technique for Breast Cancer Detection

R. Guzmán-Cabrera · J. R. Guzmán-Sepúlveda · M. Torres-Cisneros · D. A. May-Arrioja · J. Ruiz-Pinales · O. G. Ibarra-Manzano · G. Aviña-Cervantes · A. González Parada

Received: 16 February 2012 / Accepted: 3 October 2012

Abstract Breast cancer is the most common cause of death in women and the second leading cause of cancer deaths worldwide. Primary prevention in the early stages of the disease becomes complex as the causes remain almost unknown. However, some typical signatures of this disease, such as masses and microcalcifications appearing on mammograms, can be used to improve early diagnostic techniques, which is critical for women's quality of life. X-ray mammography is the main test used for screening and early diagnosis, and its analysis and processing are the keys to improving breast cancer prognosis. As masses and benign glandular tissue typically appear with low contrast and often very blurred, several computer-aided diagnosis schemes have been developed to support radiologists and internists in their diagnosis. In this article, an approach is proposed to effectively analyze digital mammograms based on texture segmentation for the detection of early stage tumors. The proposed algorithm was tested over several images taken from the digital database for screening mammography for cancer research and diagnosis, and it was found to be absolutely suitable to distinguish masses and microcalcifications from the background tissue using morphological operators and then extract them through machine learning techniques and a clustering algorithm for intensity-based segmentation.

R. Guzmán-Cabrera (✉) · M. Torres-Cisneros · J. Ruiz-Pinales · O. G. Ibarra-Manzano · G. Aviña-Cervantes · A. G. Parada
División de Ingenierías del campus Irapuato-Salamanca, Universidad de Guanajuato, Carretera Salamanca-Valle de Santiago Km 3.5+1.8 Km Comunidad de Palo Blanco, 36885 Salamanca, GTO, Mexico
e-mail: guzmanc@ugto.mx

J. R. Guzmán-Sepúlveda · D. A. May-Arrioja
Unidad Académica Multidisciplinaria Reynosa-Rodhe, Universidad Autónoma de Tamaulipas, Carretera Reynosa-San Fernando cruce con canal Rodhe, Colonia Arco iris, 88779 Reynosa, TAMPS, Mexico

Published online: 27 October 2012

Keywords Breast cancer · Detection · Mammography · Segmentation

1 Introduction

One in every eight deaths worldwide is caused by cancer. Cancer is the second leading cause of death in developed countries and the third leading cause of death in developing countries. In 2009, about 562 340 Americans died of cancer, more than 1500 people a day. Approximately 1 479 350 new cancer cases were diagnosed in 2009. In the United Sates, cancer is the second most common cause of death and accounts for nearly 1 in every 4 deaths [1]. Furthermore, breast cancer is the most common cause of death in women and the second leading cause of cancer deaths worldwide (after lung cancer) [2], and the chance of developing invasive breast cancer at some time in a woman's life is about 1 in 8 (12.5 %) [3]. Approximately 182 000 new cases of breast cancer are diagnosed and 46 000 women die of breast cancer each year in the United States [4].

Until now, there is no effective way to prevent the occurrence of breast cancer. Therefore, as it is well known, early detection is the first crucial step towards breast cancer diagnosis and treatment. In terms of medical diagnosis and screening techniques, X-ray mammography is currently the most common technique used in clinical practice due to its low cost and accessibility. Although screening mammography presents some limitations, such as low reliability on dense breast of young women or women who underwent a surgical intervention, it has been recommended as the most effective method for early detection of breast cancer as it provides high sensitivity on fatty breast and excellent performance on microcalcification detection [5]. As a result, a large number of mammograms need to be examined by a limited number of radiologists, resulting in misdiagnoses due to human errors by visual fatigue.

To improve the accuracy and efficiency of mammogram examination, computer-aided diagnosis (CAD) has been introduced in the screening process to support radiologists and internists in their diagnosis. In general, CAD systems are used to support the interpretation of medical images and two main schemes can be found: computer-aided detection (CADe) and computer-aided diagnosis (CADx); CADe is focused on the identification of the location of suspect regions while CADx is targeted to characterization (i.e., malignancy versus benignity) [2]. Currently, several image-processing methods for the detection of tumors in mammograms have been proposed. Various technologies such as fractal analysis [6], discrete wavelet transform, and Markov random field have been used. Li et al. [7] proposed a multiple circular path convolution neural network architecture that has been designed for the analysis of tumor and tumor-like structures, and Chan et al. [8] reported a two-stage adaptive density-weighted contrast enhancement algorithm for tumor detection in mammograms.

It is well known that the best prevention method is early detection, but primary prevention in early stages of the disease becomes complex as the causes remain almost unknown. Nevertheless, some typical signatures of this disease can be targeted such as masses and microcalcifications appearing on mammograms, which can be used to improve early diagnostic techniques. As a result, most of the previously mentioned techniques focused on two types of breast cancer: microcalcifications and masses.

In this study, a CADe scheme is proposed to effectively analyze digital mammograms based on texture segmentation for the detection of early stage tumors. The proposed algorithm was tested over several images taken from the digital database for screening mammography for cancer research and diagnosis, and it was found to be absolutely suitable to distinguish masses and microcalcifications from the background tissue using morphological operators and then extract them through machine learning techniques and the clustering algorithm for intensity-based segmentation.

2 Method

The main purpose of a breast cancer CADe scheme is to separate suspicious regions that may contain masses from the background parenchyma (i.e., the characteristic tissue of an organ, which is distinguished from associated connective or supporting tissues) [3–7]. In other words, such schemes divide the mammogram into several non-intersecting regions and then extract regions of interest where suspicious mass candidates from the ultrasound image can probably be found. As explained in [2], architectural distortion, which produces alterations on the density, shape, and margins, is a reliable indicator of malignant changes, especially when it is manifested through visible lesions such as mass, asymmetry, or microcalcifications. Thus, image segmentation is essential to preserve the sensitivity and accuracy of the entire mass detection and classification system.

The proposed technique is based on feature extraction through texture analysis for the identification and discrimination of suspicious areas related to cancer and benign tumors, as well as microcalcifications. As texture-based analysis methods characterize texture in terms of the extracted features, segmentation depends not only on the images under study but also on the aim for which the image texture analysis is used [6].

The performance of various methods reported in the literature has been measured on different data sets, and it has also been demonstrated that the database by itself significantly influences the performance of the algorithms [5]. The proposed algorithm deals with eight-bit gray scale images obtained from the digital database for screening mammography (DDSM) [9,10]. Abnormalities in the breast tissue, whether benign or malign, are typically found in the form of clusters of cells, which in the image means that abnormalities are represented by regions with their own properties and, in an early stage of the examination, these areas are just slightly different from the rest of the image. These texture and morphological differences in the abnormality region allow identification, analysis, discrimination, and extraction of the abnormal region. Nevertheless, such abnormal regions are not always clear to the naked eye and the aid of a more powerful tool is highly convenient.

Once it has been segmented, an image can be represented in two different ways: external and internal. External representation is used when desired shape characteristics are to be highlighted while internal representation is useful to focus on regional properties (i.e., texture and color) [11]. In the case of CAD systems, external representation is suitable to successfully diagnose the segmented regions through the analysis of morphological and geometrical properties. In this particular case, a CADe system is being proposed to identify abnormal regions within mammograms. This implies

that we are mainly focused on the internal representation as our purpose is the separation (extraction) of the objects of interest from the background based on texture segmentation (abnormalities).

The concept of transition regions, which refers to those regions located between the background and the object of interest, was first reported by Gerbrands, in 1988 [12]. From that moment a large number of studies have included this concept into image processing, especially into image segmentation. According to the definitions found in the literature, the following are the three main properties of the transition regions, which have to be taken into account for our purpose [12,13]:

The transition regions have a certain width consisting of several pixels, even around step edges.

The transition regions cover around the objects as they represent the boundary between the objects and the background.

Changes in the gray scale at the transition regions, which are frequent and diverse in real medical images, contain essential information on the transition regions themselves.

According to the properties of the transition regions, especially the one referring to the several changes in the gray scale in a single transition region, it can be stated that entropy-based algorithms exhibit a more efficient performance in terms of texture segmentation instead of gradient-based algorithms [13].

Entropy, which is, in general, a statistical measure of randomness, was first defined to be used in image processing by Pun, in 1980 [14]. Despite several proposals to consider both high-order histograms and entropies of new images generated from the properties of the original input image to obtain additional information [15], the proposed algorithm only considers the first-order entropy, which makes it easier to implement and computationally cost effective.

The definition of entropy proposed by Pun was based on Shannon's theory of communication, and it considers the operation over the full image as it is calculated from the first-order histogram, returning a scalar value as a measure of the image texture. In this particular case, we have drawn on the local entropy as the first stage of the proposed algorithm. Unlike the entropy proposed by Pun, the local entropy is defined for a small region Ω_k by a window size $(M_k \times N_k)$ within the input image, as follows: [11,13]

$$E(\Omega_k) = -\sum_{i=0}^{L-1} P_i \log(P_i), \tag{1}$$

where

$$P_i = \frac{n_i}{M_k \times N_k} \tag{2}$$

is the probability of gray scale $\boldsymbol{i}$ that appears in the neighborhood Ω_k and n_i is the number of pixels with gray scale $\boldsymbol{i}$ in the neighborhood. L is the maximal gray scale, and $E(\Omega_k)$ is the local entropy of the neighborhood Ω_k.

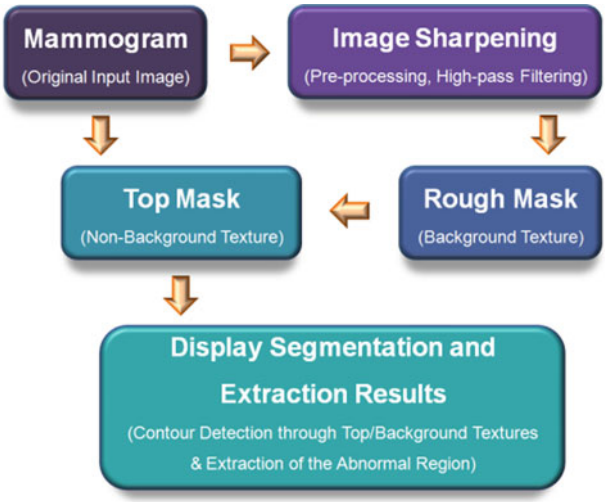

Fig. 1 General schematic of the proposed algorithm

Figure 1 shows the main stages of the proposed algorithm: input image sharpening, identification of the background texture, identification of the object's texture, and display of the results. As can be noticed in the block diagram, the regions of interest are identified and then extracted using both the original input image and the background texture as a contrast mask. This means that what it is identified as an abnormal region in the top mask stage depends on what was previously identified as the background region in the rough mask stage.

In this sense, understanding that image sharpening as a pre-processing stage is used only to enhance the details in the input image, the stages related to the background/object's texture segmentation and extraction become the most important within the process. They will be further explained in more detail.

Figure 2 shows the internal structure of the stage where the background texture is identified and then extracted. The process in this stage starts with the calculation of the local entropy of the image using Eqs. 1 and 2. This stage has two inputs: the high-pass filtered image and the gray value of the threshold. The latter is an input variable of the global process. According to the first-order processing mentioned above, a window size of 9×9 was used to compute the local entropy and then extract the properties of the local textures based only on the adjacent (surrounding) neighbors of the current pixel of the image. The next stage consists of obtaining a binary image via thresholding.

Once the image has been thresholded, a primitive version of the background texture mask is available. However, this image cannot be used for further processing yet. It is worth mentioning that after thresholding, the image remains as a binary image, which means that the textures are treated as binary region masks instead of treating them as gray scale regions.

Consequent stages constitute the morphological treatment of the image and determine the final version of the background texture. The area opening stage consists of

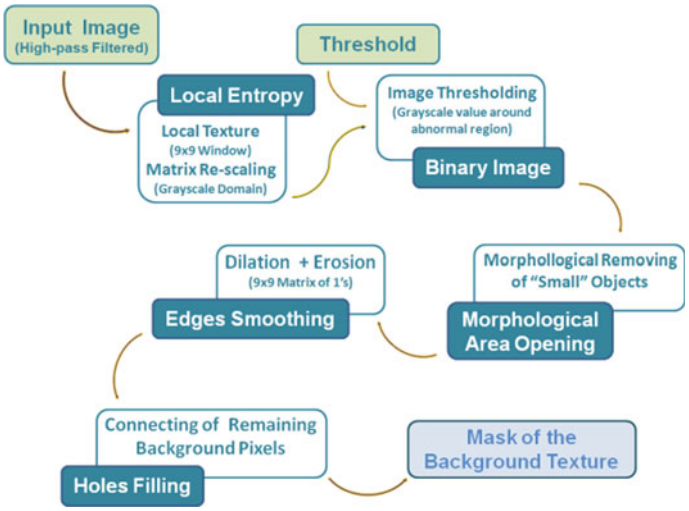

Fig. 2 Internal structure of the stage where the background texture is extracted

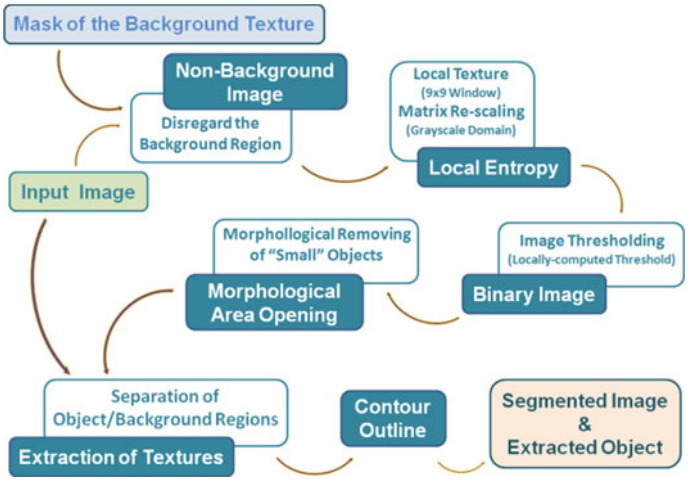

Fig. 3 Internal structure of the stage where the object's texture is extracted

removing the "small" objects from the binary image to clean the background texture. To follow the transition regions more approximately, edge smoothing is performed by a sequential process of dilation followed by erosion using a square mask of dimensions 9×9. Finally, isolated background pixels are connected by filling the holes within the background texture. Once this process has been completed, a binary image containing the background texture mask is available for further stages. The background texture mask obtained at the end of this stage is only a partial result that will be used for further processing.

The next stage, in which the object's texture is identified and then both the background and object's textures are separated, has two inputs: the original input image

and the binary image of the background mask obtained in the previous stage. Figure 3 shows the internal process of this stage, which starts using the binary image resulting from the previous stage to obtain an image containing non-background information. Texture analysis is performed over the non-background region by computing the local entropy with a similar window as that used in the previous stage. The disregarded region of the original image (background) does not contribute to further results as the local entropy is minimal for regions consisting of pixels with the same gray value [15].

Unlike the previous stage, the thresholding of the non-background region in the current stage is performed using a locally computed threshold considering the image where the background is disregarded. The morphological treatment of the binary image obtained after thresholding is similar to that performed in the previous stage. Once the binary mask of the object's texture is obtained, both regions and their contours can be reconstructed and displayed.

3 Test and Results

This section details the results of the automatic detection of a breast cancer mass in mammograms using machine learning techniques and clustering. In this analysis, the first procedure consists of determining the seed regions. When dealing with mammograms, it is known that pixels of tumor regions tend to have the maximum allowed digital value. Based on this information, morphological operators such as dilation and erosion are used to detect possible clusters which contain masses [16–19]. Image features are then extracted to remove clusters that belong to background or normal tissue as a first cut. Features used here include cluster area and eccentricity.

The images studied in this study belong to the DDSM database [9, 10]. These images are already analyzed, classified, and hand-labeled, but they are still a good indicator of the adequacy and effectiveness of the proposed algorithm. Figure 4 shows the main results of the segmentation and extraction process. Figure 4a shows the original

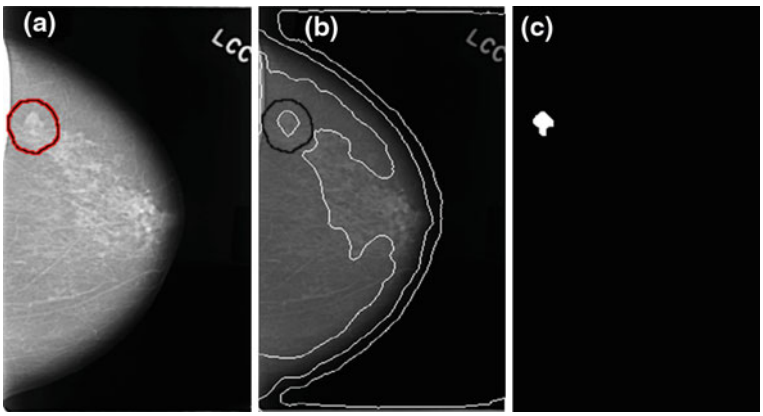

Fig. 4 Successful segmentation and extraction processes: (a) original image, (b) segmented image, and (c) extracted image. Volume 02 – Case 0018 – Left CC [9, 10]

image, which is already labeled in the abnormality region, while Fig. 4b and c shows the segmented and extracted images, respectively, for a specific relative gray level of 0.78.

The extracted abnormality shown in Fig. 4c has an area of 216 pixels while the hand-labeled region has an area of ~250 pixels (in the data set). A measure of efficiency for the proposed algorithm arises when the extracted region and the original hand-labeled region are compared to each other and to the original image using the following expressions:

$$e_{\mathrm{r}} = \frac{|A_{\text{Hand-marked}} - A_{\text{Extracted}}|}{A_{\text{Hand-marked}}} \times 100\,\% \tag{3}$$

$$e_{\mathrm{t}} = \frac{|A_{\text{Hand-marked}} - A_{\text{Extracted}}|}{A_{\text{Total}}} \times 100\,\% \tag{4}$$

Equation 3 relates the area of the hand-labeled region directly to the extracted area, without considering the size of the original image. On the other hand, Eq. 4 calculates the difference between the relative areas (i.e., hand-labeled and extracted) with respect to the total size of the original image. In this particular case, from Eq. 3, a relative error of about 13.6 % is generated after the segmentation and extraction processes with respect to the hand-labeled area are done. On the other hand, considering the total size of the original image (359 × 205 pixels), the extracted area is a good match to the hand-labeled region as they represent 0.29 % and 0.33 % of the total area of the original image, respectively, which means that, from Eq. 4, an error of ~0.04 % is generated for the extracted region with respect to the complete original image.

As explained in the previous section, two main parameters define the segmentation and extraction processes: the relative gray level of the pixels in the abnormality region and the size of the reference region for the "small" areas to be removed from the binary texture image. According to these two parameters, a successful or unsuccessful detection of the abnormality can be performed, which means that even though the segmentation is performed and the different textures are identified, it is possible that the extraction will not be carried out satisfactorily and no cluster of suspicious cells can be discriminated.

Furthermore, it was found that it is also possible for the proposed algorithm to identify suspicious regions that were not labeled in the DDSM images, as shown in Fig. 5. This does not mean that there is necessarily another abnormal region, but it means that a region with similar texture as that labeled was found; it will be the role of a radiologist or analyst to find the relevant evidence through the pertinent tests and then to diagnose the identified additional texture.

In a similar way to the previous case, the extracted region of the well-identified abnormality has an area of 696 pixels while the hand-labeled region has an area of ~650 pixels, which means that, from Eq. 3, a relative error of ~7 % is generated after the segmentation and extraction processes for a reference relative gray level of 0.73. On the other hand, the additional region that was found has an area of 125 pixels and is located slightly out of the hand-labeled region. As in the previous case, considering the total size of the original image (364 × 238 pixels), the extracted area is in good agreement with the hand-labeled region as they represent 0.8 % and 0.75 % of the total

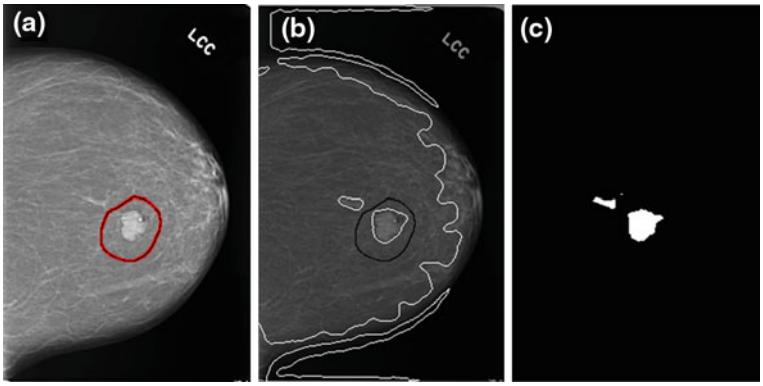

Fig. 5 Successful segmentation and extraction processes in addition to the identification of another region with similar texture: (a) original image, (b) segmented image, and (c) extracted image. Volume 02 – Case 0082 – Left CC [9,10]

area of the original image, respectively, which means that, from Eq. 4, an error of ∼0.05 % is generated for the extracted region with respect to the complete original image.

In both cases, the error is mainly produced at the stage of the algorithm where the edges are smoothed. Edge smoothing is performed by creating diamonds as the morphological structuring elements to better preserve the structural original properties of the elements in the image but it can also be performed using other geometries (i.e., square, rectangle, disk, or octagon, among others). These other geometries may produce a smaller error but the structural properties will be altered in a greater way than when diamonds are used: diamonds allow preserving the original structural properties in the extracted abnormality so this region is not only identified but it also maintains most of the original form.

In terms of the reference gray level, it was observed from the experimental results that this value strongly determines the amount of area that is identified and then extracted. Figure 6 shows the segmented and extracted images for reference gray levels of 0.77, 0.80, and 0.83. It can be clearly noticed that as the reference gray value increases, the amount of extracted area decreases but also that a cleaner extraction of the abnormality in the hand-labeled area is performed.

In a similar way to both previous cases, the hand-labeled region has an area of ∼2533 pixels. For reference gray levels of 0.77, 0.80, and 0.83, extracted areas of 2412 pixels, 970 pixels, and 328 pixels were obtained, which means that, from Eq. 3, relative errors of approximately 4.8 %, 61.7 %, and 87 % are generated after the segmentation and extraction processes, respectively. Taking into account the total size of the original image (189 × 365 pixels), the extracted areas represent 3.5 %, 1.41 %, and 0.48 % from the total image, while the hand-labeled area represents 3.67 %, which means that, from Eq. 4, errors of approximately 0.17 %, 2.26 %, and 3.19 % are generated for the extracted region with respect to the complete original image. It is significant to highlight that although the texture of the abnormality region is successfully

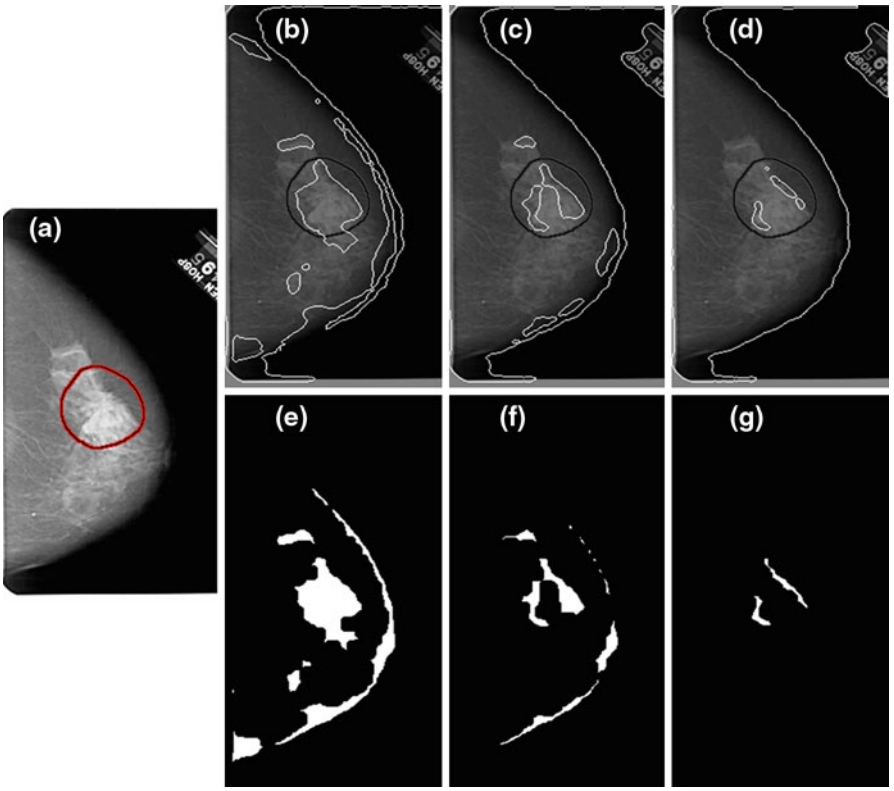

Fig. 6 Segmentation and extraction for several reference gray levels: (a) original image. Segmented images for reference gray levels: (b) 0.77, (c) 0.80, and (d) 0.83. Extracted images for reference gray levels: (e) 0.77, (f) 0.80, and (g) 0.83. Volume 11 – Case 1236 – Right CC, [9,10]

identified and extracted, results shown in Fig. 6 reflect the strong sensitivity of the algorithm to the value of the reference gray level.

From the obtained results, it can also be clearly noticed that large errors result from the direct comparison between the extracted and hand-labeled regions (i.e., Eq. 3). This is due to the small size of the concerned regions, which means that very small differences between the extracted and hand-labeled regions will result in large errors. If both region (the extracted and the hand-labeled) are referred to the total size of the original image (i.e., Eq. 4), it is clear that the error decreases. Equation 4 allows performing a more objective comparison between the extracted and the hand-labeled regions as it considers how small the abnormal region is when compared to the total size of the original image.

Figure 7 shows the evolution of the relative error as obtained from Eq. 4 for the three previous cases having several reference gray levels. In terms of the size of the extracted region, as it is also shown in Fig. 6, as the reference gray level increases, the amount of extracted area decreases; it was found from Fig. 7a and c that it decreases with approximately a quadratic dependence on the reference gray value. In the particular case of

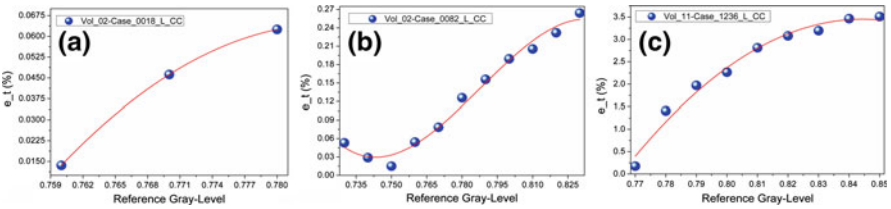

Fig. 7 Evolution of the relative error with respect to the original size of the image (Eq. 2): (a) volume 02 – Case 0018 – Left CC [9,10], (b) Volume 02 – Case 0082 – Left CC [9,10], and (c) Volume 11 – Case 1236 – Right CC [9,10]

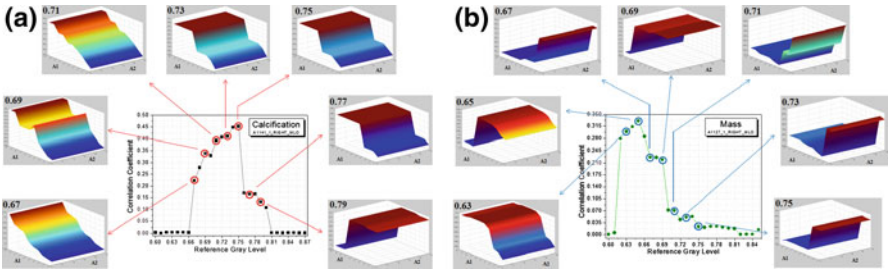

Fig. 8 Surface of the correlation coefficient between the detected area and labeled image for different gray levels in (a) microcalcification and (b) mass

Fig. 7b, the algorithm first extracted a larger region than that of the hand-labeled region and then behaves in a similar way to the other two studied cases (i.e., as the reference gray level increases, the extracted area decreases). This allows estimating the value of the reference gray level for which the extracted area becomes approximately the same as the hand-labeled area, and thus, optimizing the processing for a particular region where the abnormality has been identified.

The central graph in Fig. 8 shows the correlation coefficient between the area detected by our algorithm and the area in the labeled image for different gray levels while the reference area remains constant. By changing only the reference gray level, a filter-like response is obtained for the correlation coefficient, which means that there are specific gray levels for which a greater similitude between the processed and labeled images is achieved. To understand the effect of each variable involved in the process, a characterization of the reference area is performed for several reference gray levels.

The insets in Fig. 8 show the correlation coefficient between the identified abnormality and the labeled image as a surface that is now a function of the reference areas. Several regions can be identified on the surface, and the most adequate input parameters resulting in the highest correlation coefficient can be now set for a particular gray level. Figure 8a shows the correlation for microcalcifications, while Fig. 8b shows the correlation for the mass. By comparing Fig. 8a and b, a different behavior in the slope of the correlation curve for the case of microcalcifications and masses can be observed.

4 Conclusions

Breast cancer is one of the major causes of death among women. Early diagnoses through regular screening and timely treatments have been demonstrated as the best prevention method for cancer. In this article, we have presented a novel approach to identify the presence of breast cancer mass in mammograms. The proposed study utilizes morphological operators for segmentation and clustering for clear identification of abnormalities such as masses and microcalcifications.

Our results show that for lower values of the reference gray level, most of the abnormality is identified and extracted, but some other regions with similar textures also appear. On the other hand, for larger values of the reference gray level, these regions with similar textures gradually disappear from the image but the abnormality region is identified and discriminated with a smaller area.

According to this, an adequate value of the reference gray level is required to achieve a successful segmentation and extraction of the suspicious regions while they are discriminated in a clear and effective way, avoiding the extraction of non-relevant regions with similar textures as much as possible. In this regard, it has been demonstrated that the optimum value of the reference gray level can be estimated through the evolution of the relative error with respect to the total size of the image. Nevertheless, in terms of medical diagnostic support, this could not be the best option as it is preferable to identify suspicious regions along with non-relevant regions than to skip them and then omit important information related to possible abnormal regions. The proposed algorithm allows robust and versatile processing by only adjusting the reference gray level into an appropriate threshold value for the algorithm.

The behavior exhibited by the algorithm in the optimization procedure is directly related to the size of the reference area for the small regions to be removed after segmentation. In the case of microcalcifications, it can be clearly noticed that the correlation coefficient increases when large areas are removed, which means that the information corresponding to small areas, including those where the calcifications are located, still remain in the picture; and that, in the case of mass, the correlation coefficient increases when small areas are removed, which means that the information corresponding to large areas remains in the picture and can be discriminated later. This difference can not only be used to determine the best conditions of the input parameters but also for differentiating between microcalcification and mass, resulting in an effective image analysis for convenient assistance to medical diagnosis.

References

1. M. Garcia, A. Jemal, E. Ward, M. Center, Y. Hao, R. Siegel, M. Thun, *Global, Cancer Facts & Figures* (American Cancer Society, Atlanta, GA, 2007)
2. T.M. Deserno (ed.), *Biomedical Image Processing* (Springer, Berlin, 2010)
3. http://www.breastcancer.org, *Breast Cancer Statistics* (2009)
4. H.D. Cheng, X. Cai, X. Chen, L. Hu, X. Lou, Pattern Recognit. **36**, 2967 (2003)
5. M.J. Bottema, G.N. Lee, S. Lu, Automatic image feature extraction for diagnosis and prognosis of breast cancer, in *Artificial Intelligence Techniques in Breast Cancer Diagnosis and Prognosis, Series in Machine Perception and Artificial Intelligence*, vol 39 (World Scientific Publishing Co. Pte. Ltd., Singapore, 2000), pp. 17–54

6. L. Zheng, A.K. Chan, IEEE Trans. Med. Imaging **20**, 559 (2001)
7. H. Li, B.L. Shih-Chung, Y. Wang, L. Kinnand, M.T. Freedman, IEEE Trans. Med. Imaging **21**, 139 (2002)
8. H.P. Chan, N. Petrick, B. Sahiner, Computer-aided breast cancer diagnosis, in *Artificial Intelligence Techniques in Breast Cancer Diagnosis and Prognosis, Series in Machine Perception and Artificial Intelligence*, vol 39 (World Scientific Publishing Co. Pte. Ltd., Singapore, 2000), pp. 179–264
9. M. Heath, K. Bowyer, D. Kopans, R. Moore, W.P. Kegelmeyer, The digital database for screening mammography, in *Proceedings of the Fifth International Workshop on Digital Mammography*, ed. by M.J. Yaffe (Medical Physics Publishing, Madison, Wisconsin, 2001), pp. 212–218
10. M. Heath, K. Bowyer, D. Kopans, W.P. Kegelmeyer, R. Moore, K. Chang, S. Munish Kumaran, Current status of the digital database for screening mammography digital mammography, in *Proceedings of the Fourth International Workshop on Digital Mammography* (Kluwer Academic Publishers, Dordrecht, The Netherlands, 1998), pp. 457–460
11. R.C. Gonzalez, R.E. Woods, S.L. Eddins, in *Digital Image Processing Using MATLAB* (Pearson Prentice Hall, Upper Saddle River, NJ, 2003), chap. 11
12. J.J. Gerbrands, Segmentation of noisy images, Ph.D. Dissertation, Delft University, The Netherlands, 1988
13. C. Yan, N. Sang, T. Zhang, Pattern Recognit. Lett. **24**, 2935 (2003)
14. T. Pun, Signal Process. **2**, 223 (1980)
15. Ch. Thum, Opt. Acta Int. J. Opt. **31**, 203 (1984)
16. P. Soille, in *Morphological Image Analysis: Principles and Applications* (Springer, New York, 1999), pp. 164–165
17. L. Vincent, Morphological grayscale reconstruction in image analysis: applications and efficient algorithms. IEEE Trans. Image Process. **2**, 176 (1993)
18. S.S. Basha, K.S. Prasad, Int. J. Comput. Sci. Netw. Secur. **8**, 211 (2008)
19. S.S. Basha, K.S. Prasad, Morphological image processing in bio-medical application, in *Proceedings of PCEAI-FTOMM- International Conference* (PICA, Nagpur, 2006; Bio-Medical Engineering NCBME, Mumbai, 2006)